Simulation and Experiment of a Ku-Band Gyro-TWT

Jianxun Wang, Yong Luo, Yong Xu, Ran Yan, Youlei Pu, Xue Deng, and Hai Wang

***Abstract*— Design techniques and experimental results are presented on a Ku-band TE_{11} mode gyro-traveling wave tube. The hot test of this amplifier gives more than 153-kW output power, 2.3-GHz bandwidth (14%), 41-dB saturated gain, and 20% efficiency driven by a 63 kV, 12-A electron beam with a pitch angle ($v_t v_z$) of 1.2, and velocity spread of 5%. A linear polarized TE_{11} mode input coupler is used to introduce the input power. The stability of the amplifier from oscillation, including both the operating TE_{11} mode and the backward wave TE_{21} mode, has been investigated with linear codes, nonlinear self-consistent theory, and 3-D PIC CHIPIC simulation. To suppress the potential gyro-backward wave oscillator interactions, the high frequency circuit is loaded with lossy ceramic rings. The lossy structure is optimized by nonlinear theory and 3-D PIC simulation. A low velocity spread magnetron injection gun is designed with a new structure.**

***Index Terms*— Absolute instability, gyro-TWT, high power millimeter-wave amplifier, Ku-band, lossy ceramic, magnetron injection gun (MIG), TE_{11} mode.**

I. Introduction

HIGH-power microwave and millimeter-wave sources have been extensively researched for a variety of applications, including high-resolution radars, wideband communications, dynamic nuclear polarization, and so on [1]–[3]. The gyro-traveling wave tube (gyro-TWT) is an attractive candidate for use as the transmitter power amplifier in millimeter-wave radars [4]. Gyro-TWTs not only are capable of much broader bandwidth than other high power tubes, such as gyro-klystrons, while retaining the high power at high frequency, but also can provide much higher output power even at lower frequency compared with traditional TWTs. In spite of the fact that the background theory of gyro-TWT was developed almost simultaneously or even earlier than that of the gyrotron, the first experimental tubes yielding parameters attractive for applications were elaborated upon only in the last 20 years [4]. The main problems with the realization of a gyro-TWT can be attributed to an important issue: maintaining stability to backward wave oscillation in the interaction space, while at the same time allowing for acceptable performance in the operating mode, including high overall gain, stability to local reflective oscillations, and high average power capability. In addition, the high sensitivity to electron velocity spread is also an important factor [5].

At present, the mode instability problems of gyro-TWTs are solved in [6] and [7]. He reported successful experiments based on the operation of a gyro-TWT at the fundamental cyclotron resonance with a circular waveguide having high losses along the majority of its length and relatively short unloaded output section. All of the spurious modes are suppressed by the heavily loaded interaction circuit. To increase the average power handling capability, the structure of lossy ceramic materials interspaced with metal rings is used in this paper.

Utilizing these techniques, gyro-TWT research has made significant strides in various frequency regions over the last two decades. Early 35-GHz gyro-TWT research included an experiment at the NRL, which produced 16.6-kW peak power, 20-dB saturated gain, and 7.8% efficiency with a 3-dB bandwidth of 1.5% [8]. Harmonic gyro-TWTs have been investigated at the University of California, Davis, CA, where a second harmonic gyro-TWT in the Ku-band produced 207-kW output power, 16-dB saturated gain with 12.9% efficiency, and a bandwidth of 2.1% [9]. Also at the University of California, a gyro-TWT partially loaded with dielectric produced 55-kW peak output power, 27-dB saturated gain, and a 3-dB bandwidth of 11% in the X-band frequency range [10]. At the National Tsing Hua University, Taiwan, an ultrahigh gain gyro-TWT amplifier produced 93-kW peak power, with 70-dB saturated gain, 26.5% efficiency, and a -3-dB bandwidth of 8.6% [4]. This unprecedented gain from a gyro-TWT was achieved by employing distributed wall losses to suppress spurious oscillations. University of California Davis has performed the W-Band state-of-the-art gyro-TWT with a 140-kW output power [11], [12]. Other gyro-TWT work has been performed at the University of Maryland, College Park, at 32 GHz [13], [14], and a 35-GHz spiral waveguide gyro-TWT has been demonstrated by collaboration between the University of Strathclyde, Glasgow, U.K., and the Institute of Applied Physics, Nizhny Novgorod, Russia, [15]. In addition, MIT built a 140-GHz quasi-optical gyro-TWT employing a confocal waveguide for high-order mode operation [16].

In UESTC, we have developed a high power, wideband Ku-band gyro-TWT aimed at Ku-band radar project. Since the superconductor used in our experiment was designed for a Ku-band gyro-TWT, the length of the flat section of magnetic field is only ~300 mm, which is not long enough for a Ku-band design [17]. In addition, the maximum output power of our solid-state amplifier is only ~200 W. Consequently,

Manuscript received October 14, 2013; revised December 16, 2013; accepted December 19, 2013. Date of publication April 4, 2014; date of current version May 16, 2014. This work was supported by the National Natural Science Foundation of China under Grant G051040161101040. The review of this paper was arranged by Editor M. Blank.

The authors are with the School of Physical Electronics, University of Electronic Science and Technology of China, Chengdu 610054, China (e-mail: jxunwang@gmail.com; yluo@uestc.edu.cn; xuyong01@uestc.edu.cn).

Color versions of one or more of the figures in this paper are available online at http://ieeexplore.ieee.org.

Digital Object Identifier 10.1109/TED.2013.2296552

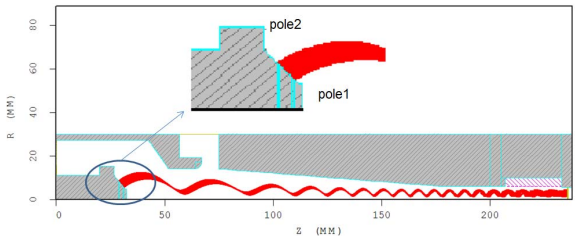

Fig. 1. Structure and beam distribution of the new-type MIG.

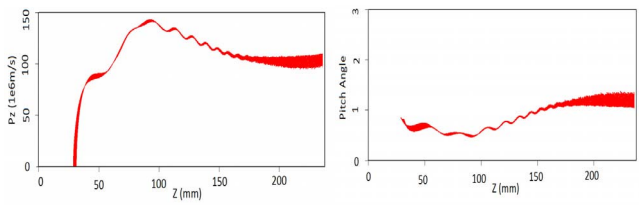

(a) (b)

Fig. 2. PIC simulation results. (a) Pz distribution. (b) Beam velocity ratio as a function of axial position.

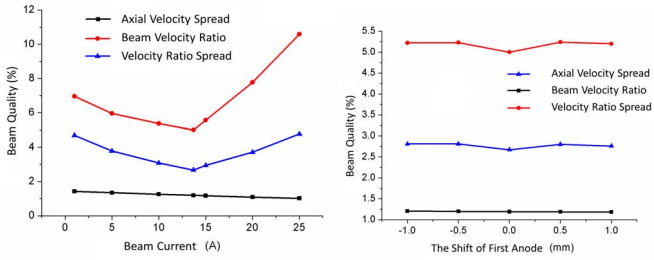

(a) (b)

Fig. 3. (a) Beam velocity ratio, beam velocity ratio spread, and v_z spread as a function of beam current. (b) Shift of first anode.

this limits the working mode selection. The TE_{01} mode can provide much higher power and it is also much easier to design the magnetron injection gun (MIG) due to the low beam density near the cathode, while the TE_{11} mode can provide much higher gain. Consequently, our gyro-TWT is designed to operate in the TE_{11} mode at the first harmonic in order to provide high gain and wide bandwidth. The beam voltage is 70 kV and the beam current is ~10 A. It is noted that in order to enhance the efficiency and gain with a short length superconductor magnet, a pitch factor of 1.2 is chosen in our design. The design of a high beam density and low magnetic field near the cathode emission area is also a challenging target. The 2-D and 3-D PIC simulations are performed by CHIPIC [18]. The new MIG structure with two focus poles is optimized by 2-D PIC simulation. The lossy ceramic rings spaced with a metal ring RF structure are used in our design to overcome the backward wave osculation. Linear theory and nonlinear theory are used to analyze the stability problems of the TE_{21} backward wave oscillation and the TE_{11} absolute instability. The beam-wave interaction is studied by numerical nonlinear calculation and 3-D PIC simulations. The simulation and cold test results of a circulator and linear polarized input coupler are also given below.

The organization of this paper is as follows. The new-type magnetron injection gun design is presented in Section II-A. Section II-B describes a circular polarized and a linear polarized TE_{11} mode coupler design. The TE_{11} and TE_{21} mode instabilities, the gyro-TWT circuit, and the loss required for the amplifier's stability are determined in Section II-C. Section II-D describes the nonlinear large-signal characteristics of the amplifier. The results of a 3-D PIC simulation of TE_{11} mode beam-wave interaction and experimental hot test are presented in Section II-E. Finally, conclusions are drawn in Section III.

II. Simulation and Experimental Study

A. Magnetron Injection Gun

The MIG gun is designed and optimized through PIC simulations. As can be seen from Fig. 1, this double anode MIG has two focus poles. The potential of the first anode is −30 kV, the cathode is −70 kV, and the second anode is 0 kV. The radius is 5 mm and the width is 4 mm. The magnetic field at the right end is 0.55 T and is ~0.065 T at the cathode emission area. The traditional MIG type is not applicable for such a low magnetic field in the emission region. As can be seen, after the electrons are emitted from the cathode, they travel a long linear distance before beginning to rotate by the magnetic field. Since in this region, the electron is not accelerated sufficiently, the velocity is low and the beam density is much higher. In the traditional design, the cathode area near the emission is nearly flat. There is no beam focus electro-static field to overcome this space charge diffusive force. Thus, it is impossible to design a high beam quality with a large beam current such as 10-A current or even higher. To overcome this problem, a new-type MIG is proposed. There are two focus poles in the both sides of the emission ring. The emitted electrons will be compressed to the beam center by the focus electrostatic field. The position and height of these two poles are optimized by PIC simulations.

Fig. 2 shows the electron axial momentum and beam pitch angle distribution with axial position at 10 ns. The rms axial velocity spread is 2.7%, and the beam pitch angle is 1.19, which satisfies the interaction design.

From Fig. 3, it can be seen that the axial speed spread is kept below 5% when the beam current is increased from 5 to 20 A when the other parameters are held constant. The velocity ratio decreased from 1.5 to 0.9. From the velocity ratio spread, which is more useful in MIG design, there is a high beam quality region when the beam current is <20 A. Also, the sensitivity property of the position of the first anode is studied. A 1-mm shift will not affect the performance significantly because of the large distance between cathode and anode.

B. Circular and Linear Polarized TE_{11} Mode Input Coupler

To increase the beam-wave interaction efficiency, the circular polarized TE_{11} mode is preferred in the first design. Unlike the two port TE_{11} coupler in [18], we designed a one port compact circular polarized TE_{11} mode input coupler as shown in Fig. 4(a). The input rectangular waveguide is divided into two different length waveguides, which are connected to the

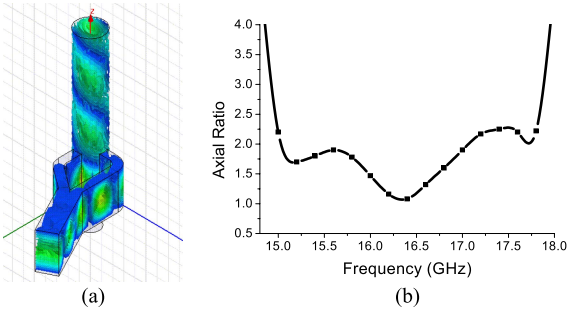

Fig. 4. Circular polarized TE_{11} input coupler. (a) Structure and HFSS simulation. (b) Axial ratio.

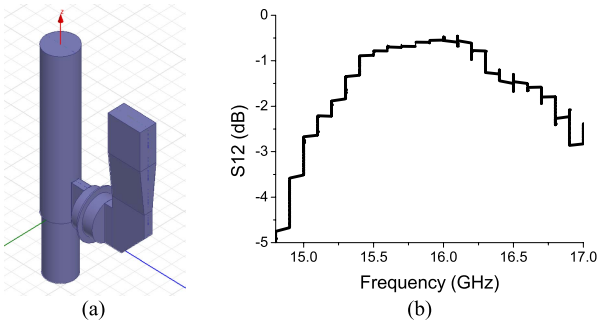

Fig. 5. Linear polarized TE_{11} input coupler. (a) Structure include pillow box window. (b) S_{21} cold test results.

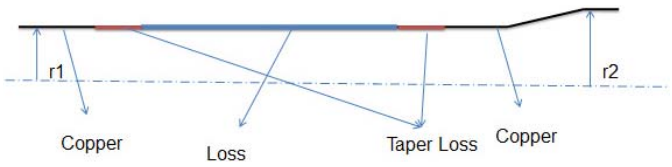

Fig. 6. Configuration of the TE_{11} mode Ku-band gyro-TWT interaction circuit.

circular waveguide with 90° difference. From HFSS simulation, the TE_{10} mode is converted to the circular polarized TE_{11} mode. The axial ratio of the excited TE_{11} mode in circular waveguide is studied. In the region between 15 and 17 GHz, the axial ratio is kept <2. The transmission parameter S_{21} is greater than −0.2 dB in this frequency band.

A linear polarized TE_{11} input coupler as shown in Fig. 5 is used in our experimental test for the simple structure. In the cold test, a pillow box-type input window is included. It provides more than 3 GHz −3-dB bandwidth, which meets the design requirement.

C. Mode Instabilities and Loss Loading

The interaction section configuration of the gyro-TWT in our experiment is shown in Fig. 6. The gyro-TWT circuit is comprised of the input coupler copper section, the loaded interaction section, the unloaded interaction section, and the linear or nonlinear output taper. The detailed design of the loading requirement in the RF circuit and mode instabilities is discussed in this section. The total length of the input coupler, the loaded interaction section, and unloaded interaction is ∼300 mm according to the length of our superconductor

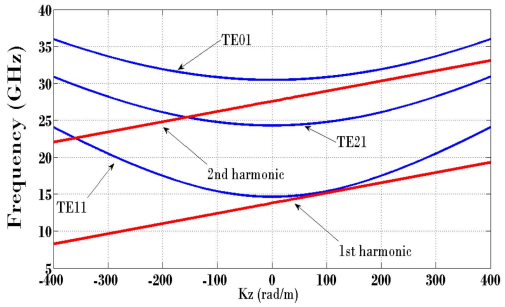

Fig. 7. Dispersion diagram of the operating mode and possible oscillating modes for the gyro-TWT.

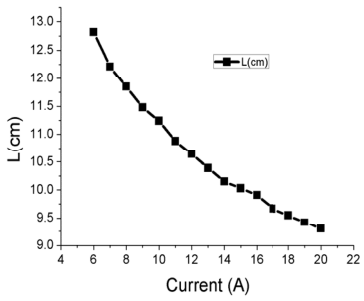

Fig. 8. Start-oscillation length versus current of TE_{21} mode.

magnet. The nonlinear, highest power portion of the amplification occurred in a short conducting wall section at the end of the interaction region.

Fig. 7 plots the diagram of the transverse electric TE_{11} and TE_{21} waveguide modes (waveguide radius is 6 mm) and the fundamental and second cyclotron harmonic beam-wave resonance lines. The magnetic field is ∼0.55 T. As it is well understood, interactions in the backward wave region are sources of absolute instabilities [5]–[7], [19]–[22]. It can be seen that second harmonic backward wave TE_{21} mode is the most probable instability mode when the beam coupling factor is included. Those interactions in the forward wave region are normally, but not always, convective instabilities. The instability of the working mode TE_{11} must also be carefully considered. The gyro-TWT is a complicated case because it exploits a convective instability near the cutoff frequency, which turns into an absolute instability at sufficiently high beam current when the unstable spectrum extends into the backward wave region.

The linear theory as described in [18] is used to study the start current, and the beam parameters including beam center and the radius of HF circuit. As shown in the f-kz diagrams the most probable oscillation mode is the TE_{21}. Linear calculations are applied to study the relationship between beam current and the start-oscillation length. Although the loss is not included, it still shows the length limitations of the last loss free section in the actual loss loaded gyro-TWT HF circuit. The beam voltage is 70 kV and the beam velocity ratio is 1.2. As shown in Fig. 8, the TE_{21} start-oscillation length is ∼100 mm with our working current if 12 A. However, considering the reflection of the output taper and window, the length of loaded section and the actual velocity ratio in

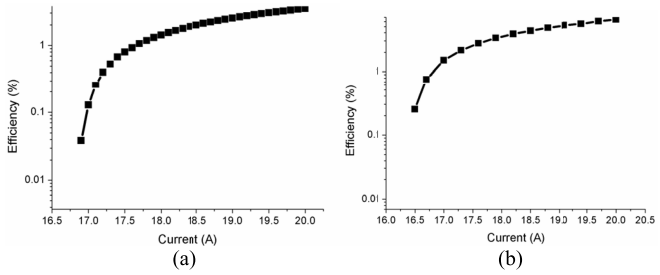

Fig. 9. Interaction efficiency of the most likely oscillating modes (a) TE_{11} and (b) TE_{21} as function of the beam current. For each mode, the oscillation starts at the beam current at which the efficiency approaches zero.

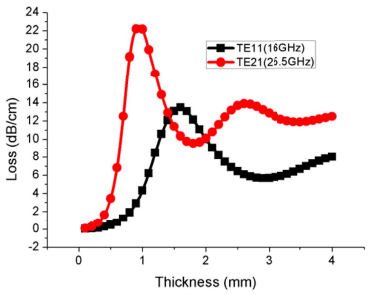

Fig. 10. Variation in cold attenuation as a function of radial dielectric thickness for the TE_{11} and TE_{21} mode at the frequency near oscillation.

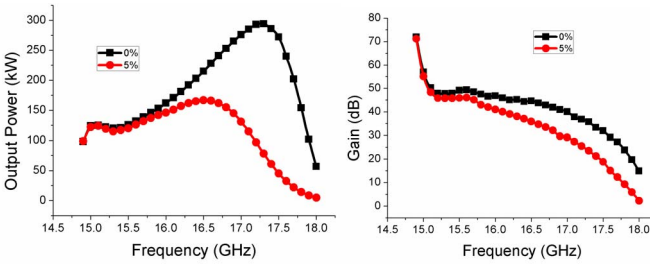

Fig. 11. Nonlinear theory calculation results with different velocity spread. (a) Efficiency as a function of frequency. (b) Saturated gain as a function of frequency.

the experiment, the loss free section of the RF circuit should be much shorter than the linear prediction. Note that this length can be determined accurately by the following nonlinear calculation and PIC simulation.

In order to accurately study the start-oscillation current, design the loss-loaded section, loss free section, and the beam-wave interaction performance, the nonlinear theory calculation is needed. The loss loaded RF circuit configuration of our Ku-band gyro-TWT is shown in Fig. 6. The start-oscillation current of the TE_{21} and TE_{11} modes is investigated by the method of interaction efficiency calculation as described in [5]. The interaction efficiency of the TE_{11} mode as a function of beam current is calculated by the nonlinear theory. The beam voltage is 70 kV and the velocity ratio is 1.2 in the calculation. The wall resistivity is 30 000 times that of ideal copper in the calculation. It can be seen from Fig. 9(a) that the start oscillation current is $\sim$17 A and the frequency is 14.9 GHz. These losses correspond to a $-$75-dB attenuation of the entire loss section. The backward wave oscillation of the TE_{21} mode is also shown in Fig. 9(b); the start oscillation current is $\sim$16 A when the wall resistivity is 10 000 times that of ideal copper. The corresponding oscillation frequency is 25.5 GHz. In this case, the total attenuation of the circuit is about $-$30 dB.

In the actual high average power tube, the high-thermal conductivity BeO-SiC lossy ceramic rings are used rather than the coated distributed-loss structure as presented in [23]. These lossy ceramic rings spaced with a metal ring RF structure have higher average power handling capability [24], and it is also much easier to control the loading of a normally propagating operating mode. Since the attenuation is dependent upon on the radius and thickness of the ceramic in electromagnetics, the variation of the attenuation dependence upon thickness is studied. A code, based on the mode matching technique, is written to calculate the hybrid waves in the vacuum and dielectric regions as shown in Fig. 10. There are several maximum attenuation positions at different thicknesses. From this result, the optimum thickness can be chosen.

D. Nonlinear Numerical Calculations

A large signal self-consistent code based on [7] that accounts for loss and the electron beam spread is used to evaluate the performance characteristics of the device. The distributed wall loss is shown in Fig. 1, the reflections from the finite mismatch of the input and output couplers and the loss taper are also included in the calculation. The amplifier parameters are given in Table I. To ensure that the wave is not damped in the high power region, there is no loss added to the final 60 mm of the circuit and the loss in the preceding 20 mm is linearly tapered.

The beam-wave interaction efficiency dependence on frequency is shown in Fig. 11 with an ideal beam and a 5% axial speed spread, which is a normal value in gyro-TWT MIG design. A circulator polarized input TE_{11} mode is assumed. Nine beamlets, each with 16 electrons, are used in our calculation; thus, 132 beams are included. The maximum output power is $\sim$300 kW with an $\sim$2.3-GHz bandwidth assuming an ideal beam. However, when the 5% spread beam is considered, the maximum output power decreased to $\sim$170 kW. Note that it is clearly seen that the output power does not decrease appreciably when the frequency is $<$16 GHz. This is because the operation is close to the cutoff region, and the wavenumber kz is very small. Consequently, the effect of the electron velocity spread is minimized. While at the frequency near 17 GHz, the output power decreased considerably because of the influence of a large wavenumber (kz). The corresponding maximum efficiency is $\sim$25%, and the $-$3-dB bandwidth is $\sim$2.3 GHz when the 5% axial speed spread is included.

E. 3-D PIC Simulation and Hot Test

In order to investigate the details of the beam-wave interaction, the 3-D particle in cell (PIC) simulation is performed. The input TE_{11} mode is linear polarized as we used in the experiment. It is injected into the circuit from the left end in the simulation. The mesh number in the radial, azimuthal, and axial direction is 37 $\times$ 52 $\times$ 348, and the total mesh number

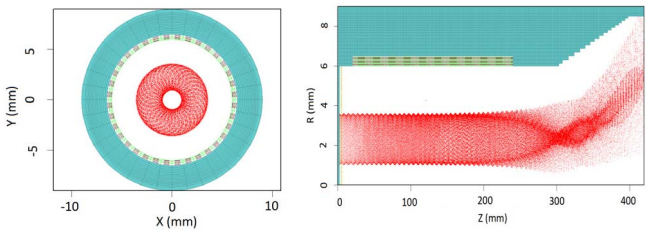

Fig. 12. 3-D PIC simulation. (a) Beam distribution in the cross section. (b) Beam distribution in the axial direction.

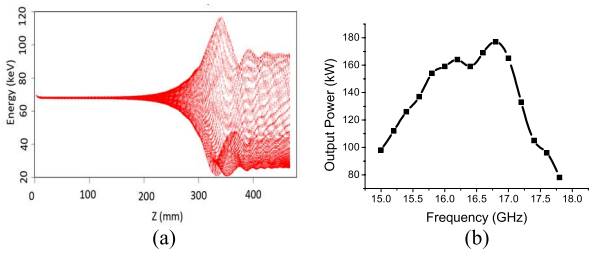

Fig. 13. (a) Beam energy distribution as a function of axial position. (b) Output power as a function of frequency.

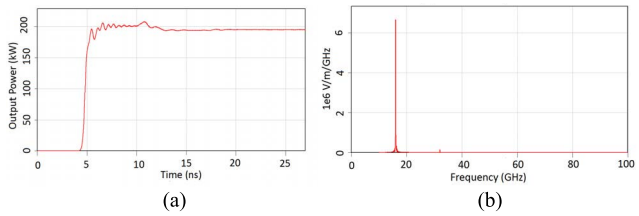

Fig. 14. Output character of the output port. (a) Output power at 16 GHz as a function of time. (b) Spectrum of the output transverse electrified.

is 669 552. More than 200 000 electrons are included in the simulation. Fig. 12 shows the beam distribution of the 3-D PIC simulation. The circuit include the input loss free section, the loss loaded section, and the output loss free section and simple linear output taper. The ideal 70 kV, 10-A beam is injected into the RF circuit from the left end. The beam center is ∼2.4 mm. It can be seen that there is a strong beam wave interaction at the output loss free section. From Fig. 13(a), it can be seen that most of the electrons lost their energy rapidly after entering the output loss free section. While there are still some electrons which gain energy, it is necessary to pay close attention to collecting of them. They can traverse a much longer distance in the axial direction. Consequently, an output window with improper position will probably be cracked by these electrons. The saturated output power as a function of frequency is shown in Fig. 13(b). The maximum output power is ∼177 kW with a 25% efficiency at 16.8 GHz. The differences between the nonlinear theory calculation and simulation results may be caused by the difference of the lossy circuit model. In addition, the space charge effect, the real axial magnetic field, and more electrons are included in the PIC simulation.

The temporal dependence of output power is shown in Fig. 14(a). The output power becomes stable at ∼6 ns.

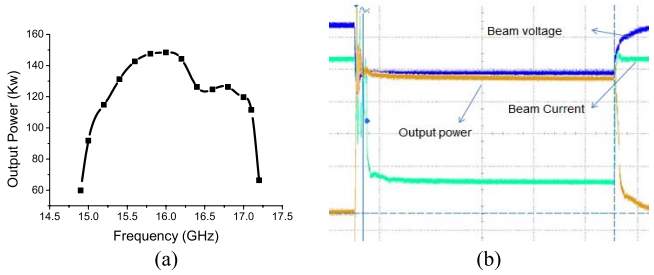

Fig. 15. Experiment hot test results. (a) Dependence of output power on frequency with 63 kV, 12-A beam. (b) Waveform of voltage, current, and output.

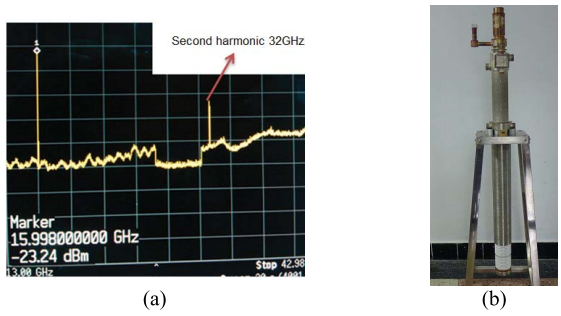

Fig. 16. Experiment hot test results. (a) Spectrum of 16-GHz input and second harmonic 32 GHz. (b) Picture of the gyro-TWT.

The spectrum of the output is also studied. It looks quite pure and there is no TE_{21} mode backward wave oscillation as shown in Fig. 14(b).

The hot test of our Ku-band TE_{11} gyro-TWT is performed. The measured beam voltage is ∼63 kV, the beam current is ∼12 A. The input power is 10 W and the gain is ∼41 dB at the frequency of 16 GHz. The recently experimental test results are shown in Fig. 15. The maximum output power 153 kW, which corresponds to 20% efficiency. This interaction efficiency is very close to the nonlinear calculation with 5% velocity spread. The −3-dB bandwidth is ∼2.3 GHz. The waveforms of the beam voltage, beam current, and output power are also given. The pulsewidth is 200 μs. Further experimental tests will be performed to study the spectrum and average power. From the spectrum test as shown in Fig. 16, the input frequency of 16 GHz and the second harmonic at 32 GHz are also observed. The picture of the Ku-band TE_{11} mode gyro-TWT is presented.

III. Conclusion

The design and experimental test of a Ku-band TE_{11} mode gyro-TWT have been described aimed at the requirement of a radar project. Linear and nonlinear theories are used to design the HF circuit and the lossy section. The input circularized TE_{11} coupler is designed with low axial ratio. The loss section is carefully designed to suppress oscillations due to the absolute instability of the TE_{11} mode and second harmonic backward oscillation of TE_{21} mode. The 3-D PIC simulations are also used to study the beam-wave interaction and stability. A new-type low velocity spread MIG is designed and optimized by 2-D PIC simulation. The hot test of the

Ku-band TE_{11} gyro-TWT is performed. The maximum output power is 153 kW, which corresponds to ∼20% efficiency at 16 GHz. The corresponding input power is 10 W corresponding to 41-dB gain with a 63 kV, 12-A beam. In addition, a 2.3-GHz (14%) bandwidth is achieved.

ACKNOWLEDGMENT

The authors would like to thank Dr. W. C. Tsai, Dr. A. Baig, and Prof. N. C. Luhmann for many useful discussions about the nonlinear theory and calculation of gyro-TWT.

REFERENCES

[1] M. Thumm, "Novel application of millimeter and submillimeter wave gyro-devices," *Int. J. Infr. Millimeter Waves*, vol. 22, no. 3, pp. 377–385, Mar. 2001.

[2] K. L. Felch, B. G. Danly, H. R. Jory, K. E. Kreischer, W. Lawson, B. Levush, *et al.*, "Characteristics and applications of fast-wave gyrodevices," *Proc. IEEE*, vol. 87, no. 5, pp. 752–781, May 1999.

[3] V. L. Granatstein, B. Levush, B. G. Danly, and R. K. Parker, "A quarter century of gyrotron research and development," *IEEE Trans. Plasma Sci.*, vol. 25, no. 6, pp. 1322–1335, Dec. 1997.

[4] K. R. Chu, H. Y. Chen, C. L. Hung, T. H. Chang, L. R. Barnett, S. H. Chen, *et al.*, "Theory and experiment of ultrahigh gain gyrotron traveling wave amplifier," *IEEE Trans. Plasma Sci.*, vol. 27, no. 2, pp. 391–404, Apr. 1999.

[5] W. C. Tsai, T. H. Chang, N. C. Chen, and K. R. Chu, "Absolute instabilities in a high-order-mode gyrotron traveling-wave amplifier," *Phys. Rev. E*, vol. 70, no. 5, pp. 056402-1–056402-8, 2004.

[6] K. R. Chu and A. T. Lin, "Gain and bandwidth of the gyro-TWT and CARM amplifier," *IEEE Trans. Plasma Sci.*, vol. 16, no. 2, pp. 90–104, Apr. 1988.

[7] K. R. Chu, Y. Y. Lau, L. R. Barnett, and V. L. Granatstein, "Theory of a wide-band distributed gyrotron traveling-wave amplifier," *IEEE Trans. Electron Devices*, vol. 28, no. 7, pp. 866–871, Jul. 1981.

[8] J. L. Seftor, V. L. Granatstein, K. R. Chu, P. Sprangle, and M. E. Read, "The electron cyclotron maser as a high-power traveling wave amplifier of millimeter waves," *IEEE J. Quantum Electron.*, vol. 15, no. 9, pp. 848–853, Sep. 1979.

[9] Q. S. Wang, D. B. McDermott, and N. C. Luhmann, "Operation of a stable 200 kW second harmonic gyro-TWT amplifier," *IEEE Trans. Plasma Sci.*, vol. 24, no. 3, pp. 700–706, Jun. 1996.

[10] K. C. Leou, D. B. McDermott, C. K. Chong, and N. C. Luhmann, "Experimental investigation of a broadband dielectric-loaded gyro-TWT amplifier," *IEEE Trans. Electron Devices*, vol. 43, no. 6, pp. 1016–1020, Jun. 1996.

[11] D. B. McDermott, H. H. Song, A. T. Lin, L. R. Barnett, T. H. Chang, K. R. Chu, *et al.*, "Design of a W-band TE01 mode gyrotron traveling-wave amplifier with high power and broad-band capabilities," *IEEE Trans. Plasma Sci.*, vol. 30, no. 3, pp. 894–902, Jun. 2002.

[12] D. B. McDermott, H. Song, Y. Hirata, A. T. Lin, T. H. Chang, K. R. Chu, *et al.*, "140 kW, 94 GHz heavily loaded TE gyro-TWT," in *Proc. 2nd Int. Vac. Electron. Conf.*, Apr. 2001, pp. 143–144.

[13] H. Guo, S. H. Chen, V. L. Granatstein, J. Rodgers, G. Nusinovich, M. Walter, *et al.*, "Operation of a highly overmoded, harmonic-multiplying, wideband gyrotron amplifier," *Phys. Rev. Lett.*, vol. 79, no. 3, pp. 515–518, Jul. 1997.

[14] G. S. Nusinovich, J. Rodgers, W. Chen, and V. L. Granatstein, "Phase stability in gyro-traveling-wave-tubes," *IEEE Trans. Electron Devices*, vol. 48, no. 7, pp. 1460–1468, Jul. 2001.

[15] V. L. Bratman, A. W. Cross, G. G. Denisov, W. He, A. D. R. Phelps, K. Ronald, *et al.*, "High-gain wide-band gyrotron traveling wave amplifier with a helically corrugated waveguide," *Phys. Rev. Lett.*, vol. 84, no. 12, pp. 2746–2749, Mar. 2000.

[16] J. R. Sirigiri, M. A. Shaprio, and R. J. Temkin, "High power 140 GHz quasi-optical gyrotron travelling wave amplifier," *Phys. Rev. Lett.*, vol. 90, no. 25, pp. 258–302, Jun. 2003.

[17] H. Wang, H. F. Li, Y. Luo, and R. Yan, "Theoretical and experimental investigation of a Ka-band gyro-TWT with lossy interaction structure," *Int. J. Infr. Millim. Waves*, vol. 32, no. 2, pp. 172–185, Feb. 2011.

[18] Z. Da-Jun and L. Sheng-gang, "Electronmagnetic field algorithms of CHIPIC code," *J. Univ. Electron. Sci. Technol. Chin.*, vol. 34, no. 4, pp. 485–488, 2005.

[19] K. R. Chu, L. R. Barnett, W. K. Lau, L. H. Chang, and H. Y. Chen, "A wide-band millimeter-wave gyrotron traveling-wave amplifier experiment," *IEEE Trans. Electron Devices*, vol. 37, no. 6, pp. 1557–1560, Jun. 1990.

[20] C. H. Du and P. K. Liu, "Linear full-wave-interaction analysis of a gyrotron-traveling-wave-tube amplifier based on a lossy dielectric-lined circuit," *IEEE Trans. Plasma Sci.*, vol. 38, no. 6, pp. 1219–1226, Jun. 2010.

[21] B. T. Liu, J. J. Feng, E. F. Wang, Z. L. Li, X. Zeng, L. J. Qian, *et al.*, "Design and experimental study of a Ka-band gyro-TWT with periodic dielectric loaded circuits," *IEEE Trans. Plasma Sci.*, vol. 39, no. 8, pp. 1665–1672, Aug. 2011.

[22] C. S. Kou, Q. S. Wang, D. B. McDermott, A. T. Lin, K. R. Chu, and N. C. Luhmann, "High power harmonic gyro-TWTs. I. Linear theory and oscillation study," *IEEE Trans. Plasma Sci.*, vol. 20, no. 3, pp. 155–169, Jun. 1992.

[23] M. Garven, J. P. Calame, B. G. Danly, K. T. Nguyen, B. Levush, F. N. Wood, *et al.*, "A gyrotron-traveling-wave tube amplifier experiment with a ceramic loaded interaction region," *IEEE Trans. Plasma Sci.*, vol. 30, no. 3, pp. 885–893, Jun. 2002.

[24] J. P. Calame, M. Garven, B. G. Danly, B. Levush, and K. T. Nguyen, "Gyrotron-traveling-wave-tube circuits based on lossy ceramics," *IEEE Trans. Electron Devices*, vol. 49, no. 8, pp. 1469–1477, Aug. 2002.

Authors' photographs and biographies not available at the time of publication.